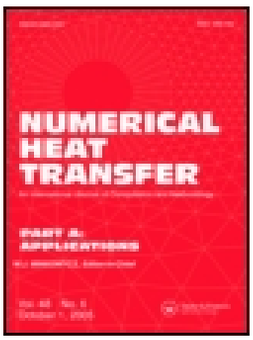

Numerical Heat Transfer, Part A: Applications

ISSN: 1040-7782 (Print) 1521-0634 (Online) Journal homepage: http://www.tandfonline.com/loi/unht20

NATURAL CONVECTION IN TRAPEZOIDAL CAVITIES WITH BAFFLES MOUNTED ON THE UPPER INCLINED SURFACES

F. Moukalled, S. Acharya

To cite this article: F. Moukalled, S. Acharya (2000) NATURAL CONVECTION IN TRAPEZOIDAL CAVITIES WITH BAFFLES MOUNTED ON THE UPPER INCLINED SURFACES, Numerical Heat Transfer, Part A: Applications, 37:6, 545-565, DOI: 10.1080/104077800274082

To link to this article: http://dx.doi.org/10.1080/104077800274082

Published online: 29 Oct 2010.

Numerical Heat Transfer, Part A, 37:545–565, 2000

1040–7782/00 $12.00 + .00

NATURAL CONVECTION IN TRAPEZOIDAL CAVITIES WITH BAFFLES MOUNTED ON THE UPPER INCLINED SURFACES

F. Moukalled
Department of Mechanical Engineering, Faculty of Engineering and Architecture, American University of Beirut, Beirut, Lebanon

S. Acharya
Mechanical Engineering Department, Louisiana State University, Baton Rouge, Louisiana, USA

A numerical investigation has been undertaken to study the effects of mounting baffles to the upper inclined planes of trapezoidal cavities (representing a building or attic space). Two thermal boundary conditions are considered: (a) the vertical and upper surfaces are heated while the lower surface is cooled (summerlike conditions); (b) the lower surface is heated while the other surfaces are cooled (winterlike conditions). For each boundary condition, computations are performed for two baffle heights and two baffle locations. Rayleigh number (Ra) values range from 10^3 to 5×10^7 for summerlike conditions and from 10^3 to 10^6 for winterlike conditions. For both boundary conditions, results obtained with air as the working fluid reveal a decrease in heat transfer in the presence of baffles. In winterlike conditions, convection starts to dominate at an Ra much lower than that in summerlike conditions. The decrease in heat transfer becomes increasingly more significant as the baffle gets closer to the heated vertical wall for the bottom-cooled situation and as the baffle gets closer to the symmetry line for the bottom-heated case. In general, this decrease in heat transfer is higher with taller baffles. Average Nusselt number (Nu) correlations for both boundary conditions are presented.

INTRODUCTION

Natural convection in rectangular enclosures and cylindrical annuli have received considerable attention in recent years [1]. On the other hand, studies dealing with natural convection in more complex geometries have been rather limited. The focus of this investigation is on natural convection in trapezoidal cavities with baffles attached to their upper inclined surfaces. The physical situation, relevant to attic spaces and industrial buildings, is schematically displayed in Figure 1*a*.

Received 10 September, 1999; accepted 7 December, 1999.

The financial support provided by the University Research Board of the American University of Beirut through Grant No. 48720 is gratefully acknowledged. Computations were performed in the Department of Mechanical and Mechatronic Engineering at the University of Sydney, Sydney, Australia. Special thanks are due to Prof. M. Masri for allowing the use of his computational facilities and to Prof. D. Fletcher for performing the FLOW-3D computations.

Address correspondence to Professor Sumanta Acharya, Louisiana State University, Department of Mechanical Engineering, 204 Thomas Boyd, Baton Rouge, LA 70803-6413, USA.

NOMENCLATURE

c_p	specific heat of fluid	x, X	dimensional and dimensionless coordinate along the horizontal direction
g	gravitational acceleration		
k	thermal conductivity		
k_b	baffle thermal conductivity	y, Y	dimensional and dimensionless coordinate along the vertical direction
k_r	dimensionless baffle conductivity		
L	height of the short vertical wall	β	coefficient of thermal expansion
Nu, Nu*	local and normalized Nusselt number	μ	viscosity
$\overline{\text{Nu}}$, $\overline{\text{Nu}^*}$	average and normalized average Nusselt number	ψ	stream function
		ρ	density
p,P	dimensional and dimensionless pressure	θ	dimensionless temperature
		θ_b	dimensionless baffle temperature
Pr	Prandtl number ($= \mu c_p/k$)		
Ra	Rayleigh number ($= g\beta(T_h - T_c)L^3/\nu\alpha$)	**Subscripts**	
S	distance along wall		
T	dimensional temperature		
u, U	dimensional and dimensionless horizontal velocity component	c	cold wall
		h	hot wall
v, V	dimensional and dimensionless vertical velocity component	i	condition at baffle-air interface
		max	maximum value

A few investigations dealing with natural convection heat transfer in triangular enclosures have been reported. This configuration may be viewed as a special case of trapezoidal cavities. Akinsete and Coleman [2] studied natural convection in a right triangular cavity with an adiabatic vertical wall and for two different boundary conditions of uniform temperature and uniform heat flux along the horizontal and inclined sides. Karyakin, Sokovishin, and Martynenko [3] obtained transient natural convection results in an isosceles triangular enclosure. Bejan and Poulikakos [4] and Poulikakos and Bejan [5, 6] studied natural convection and the associated fluid dynamics in an attic space. Their theoretical analysis revealed that, even at the highest value of Ra considered, when cooling the top inclined wall of the enclosure, the natural circulation within the cavity is composed of a single cell. Salmun [7] solved numerically the same problem using two different numerical schemes. Reported results using both schemes showed that the general flow structure corresponds to a single convective cell for low values of Ra and to multiple convective cells for high values of this parameter. Salmun [8] analyzed, using linear theory, the stability of the two-dimensional asymptotic solution to secondary flow disturbances in the same triangular cavity.

A limited number of studies also have been reported on natural convection heat transfer in undivided trapezoidal cavities. The experimental and numerical work of Iyican et al. [9, 10] dealt with an inclined trapezoidal cavity with plane adiabatic sidewalls and cylindrical top and bottom walls that are maintained at different uniform temperatures. Lam, Gani, and Symons [11] compared numerical results with experimental data in a trapezoidal cavity composed of two vertical

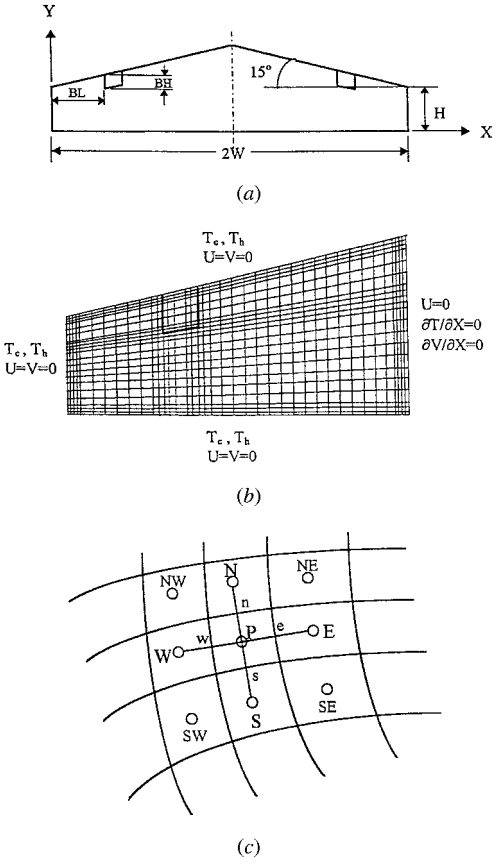

Figure 1. (*a*) Physical domain; (*b*) computational domain and an illustrative grid network; (*c*) a typical control volume.

adiabatic side walls, a horizontal hot bottom wall, and an inclined cold top wall. Their work revealed that, under the boundary conditions used, a two-dimensional numerical model is sufficient to predict heat transfer rates to an acceptable level of accuracy, but it cannot describe the three-dimensional flow field that occurs in the cavity. Karyakin [12] performed a study on transient natural convection in prismatic enclosures of arbitrary cross section and presented results for transient natural convection in a trapezoidal cavity with parallel top and bottom walls and inclined side walls. Lee [13] presented numerical results for laminar natural convection in trapezoidal cavities with horizontal adiabatic bottom and top walls and isothermal inclined side walls that are maintained at two different temperatures. Peric [14] conducted a study similar to that of Lee and concluded that Lee's results were not accurate. Computations in the same geometry were carried out by Sadat and Salagnac [15] using a control volume based finite element technique for values of

Ra ranging from 10^3 to 2×10^5, and by Kuyper and Hoogendoorn [16], using the control volume method for Ra between 10^4 and 10^8.

Recently, Moukalled and Acharya [17] reported on natural convection heat transfer in a partially divided trapezoidal cavity with the partial divider being attached to the lower horizontal base of the cavity. For both boundary conditions used, results presented showed that the presence of baffles decreases heat transfer. The intent of this paper is to extend the work reported in [17] into situations where the partial dividers are attached to the upper inclined plane of the cavity. No previous work on this geometry has been reported.

PHYSICAL MODEL AND GOVERNING EQUATIONS

The physical model for the study, representing an attic space or an industrial building, is sketched in Figure 1*a*. Two boundary conditions are considered. In the first, the bottom wall of the cavity is maintained at a uniform cold temperature T_c and all other walls are maintained at a uniform hot temperature T_h. This boundary condition simulates summerlike conditions in the attic, with the vertical and top walls exposed to the hot ambient and the lower surface exposed to the air-conditioned interior at a lower temperature. In the second, the bottom wall is hot (T_h) while the temperature of all other walls is T_c. This configuration is equivalent to wintertime conditions in the attic with the vertical and top walls exposed to the cold ambient and the lower surface adjoining the heated interior of the building. In both cases, the effects of mounting two symmetrically located baffles or partial dividers to the top inclined wall of the cavity on the amount of heat transferred to or from an adjacent space are studied. Because of symmetry around the y-axis, computations are performed in only half of the physical domain.

In the configuration studied, the width of the cavity (W) is four times the height (L) of the short vertical wall. The inclination of the top of the cavity is fixed at 15 degrees. Two baffle heights (BH $= H/3$ and $2H/3$, where H the cavity's height at the baffle location) and two baffle locations (BL $= W/3$ and $2W/3$) are considered. In all computations, the baffle thickness (BT) is taken as BT $= W/20$ to simulate a thin baffle.

The flow is assumed to be laminar, steady, and two dimensional. The fluid properties are considered to be constant except for the variations of density in the body force term, which are represented by the Boussinesq approximation. The governing equations are nondimensionalized using the following dimensionless variables:

$$X = \frac{x}{L} \qquad Y = \frac{y}{L} \tag{1}$$

$$U = \frac{u}{v/L} \qquad V = \frac{v}{v/L} \tag{2}$$

$$P = \frac{P + \rho g y}{\rho (v/L)^2} \qquad \theta = \frac{T - T_c}{T_h - T_c} \tag{3}$$

With the above-stated assumptions, the dimensionless governing transport equations of mass, momentum, and energy are, respectively.

$$\vec{\nabla} \cdot \vec{V} = 0 \tag{4}$$

$$\vec{V} \cdot \vec{\nabla} U = -\vec{i} \cdot \vec{\nabla} P + \vec{\nabla} \cdot (\vec{\nabla} U) \tag{5}$$

$$\vec{V} \cdot \vec{\nabla} V = -\vec{j} \cdot \vec{\nabla} P + \vec{\nabla} \cdot (\vec{\nabla} V) + \frac{\mathrm{Ra}\,\theta}{\mathrm{Pr}} \tag{6}$$

$$\vec{V} \cdot \vec{\nabla} \theta = \frac{1}{\mathrm{Pr}} \vec{\nabla} \cdot (\vec{\nabla} \theta) \tag{7}$$

In the baffle region, since the velocity field vanishes, the governing conservation equations reduce to the Laplace equation, and the dimensionless temperature distribution can be expressed as

$$\frac{k_r}{\mathrm{Pr}} \vec{\nabla} \cdot \left(\vec{\nabla} \theta_b \right) = 0 \tag{8}$$

where k_r is the ratio between the thermal conductivity of the baffle and the thermal conductivity of the fluid, and θ_b denotes the nondimensional temperature in the baffle. The energy balance at the baffle–air interface can be stated as

$$-\frac{1}{\mathrm{Pr}} (\vec{n} \cdot \vec{\nabla} \theta)_j = -\frac{k_r}{\mathrm{Pr}} \left(\vec{n} \cdot \vec{\nabla} \theta_b \right)_i \tag{9}$$

where $\vec{n}$ is a unit vector in the direction normal to the baffle–air interface and the subscript i refers to the interface.

The associated flow and thermal boundary conditions (Figure 1*b*) are the no-slip condition on the enclosure walls and nondimensional uniform temperatures of 1 and 0 along the hot and cold walls, respectively. Along the vertical symmetry line, the normal temperature gradient, the normal V-velocity gradient, and the U-velocity all are set to zero.

SOLUTION PROCEDURE

The coupled system of equations governing the flow and temperature fields (Eqs. (4)–(7)) is solved numerically using the control volume approach. A nonstaggered curvilinear grid arrangement is used and the method of Rhie and Chow [18] that embodies the SIMPLE algorithm of Patankar [19] is employed to suppress oscillatory checkerboard fields. In this method, the solution domain is divided into a number of control volumes, each associated with a grid point (Figure 1*c*). The discretized form is obtained by first expressing Eqs. (4)–(7) using a general curvilinear coordinate system and then integrating the resulting equations over the control volume shown in Figure 1*c*, along with suitable interpolation for the variables whose values are unknown on the control volume faces. In this paper,

power law profile approximations [19] are made in each coordinate direction. This reduces the system of differential equations to a system of algebraic equations, which is then solved iteratively using a line-by-line Thomas algorithm. Pressure–velocity coupling is resolved through a guess-and-correct procedure similar to that described by Patankar [19].

The grid is generated using an algebraic method known as "transfinite mappings" or "transfinite interpolations" [20, 21, 22]. In this approach, the mapping is done using a bilinear shape function very similar to a finite element shape function. However, a special procedure is used to calculate the local coordinates of each internal grid point as a weighted function of the corresponding boundary points along each local coordinate direction. The local coordinates are obtained from a linear interpolation procedure between the opposite boundary nodes. An illustrative grid network generated is shown in Figure 1*b*.

The presence of the divider in the calculation domain is accounted for by the special treatment suggested by Patankar [19]. In this strategy, the conservation equations (4)–(7) are solved in the whole domain, with the coefficients of the momentum equations at the main grid points in the baffle set to a very high value ($\sim 10^{30}$) and the dimensionless divider conductivity set to k_r/Pr. These specifications in addition to the no-slip boundary condition suppress the velocities in the baffle to vanishing values and reduce Eq. (7) to the appropriate Laplace equation (Eq. (8)). Energy balance at the baffle–air interface is ensured by arranging the control volume faces to coincide with the divider interface. Since a conservative numerical scheme is being used, energy into and out of the divider interface are equal and Eq. (9) is satisfied.

Numerical Accuracy

All computations were performed on a 120×120 nonuniform mesh system. As shown in Figure 1*b*, grid points were concentrated near all solid surfaces where large gradients of the flow variables were expected. The final grid was chosen after comparing the computed profiles of velocity, temperature, and the local Nu for a number of grid sizes. A comparison between the solution presented in this paper and that generated on a 160×160 nearly uniform grid revealed a maximum difference in the various predicted quantities to be smaller than 0.69%. Conservation for the various physical quantities was satisfied to within 0.001% in each control volume. Evaluation of the solution accuracy also was made by comparing the results with those generated on an identical grid using the well-known FLOW-three-dimensional commercial CFD code. The difference in the average Nu for the cases studied was less than 0.05%. A three-dimensional version of the problem also was solved for a few cases using FLOW-3D for the bottom-cooled boundary condition representing summer. The maximum difference in the average Nu between the two- and three-dimensional computations was within acceptable limits (less than 5.84%). In fact, streamline plots revealed that the problem is primarily two dimensional. As a further check for accuracy, computations were performed for a nonpartitioned trapezoidal cavity using the boundary conditions of Lam et al. [11], and excellent agreement was found with their surface heat transfer results.

RESULTS AND DISCUSSION

The governing parameters in the problem are the Prandtl number (Pr), the Ra, the conductivity ratio (k_r), the divider depth (BH), and the divider location (BL). To reduce the number of parameters involved, the Pr is assigned the value of 0.72 corresponding to air and k_r is fixed at 2 to simulate a poorly conducting divider. Results are obtained for two baffle heights (BH $= H/3$ and $2H/3$), two baffle locations (BL $= W/3$ and $2W/3$), and Ra values varying between 10^3 and 5×10^7 for the summertime boundary condition and between 10^3 and 10^6 for the wintertime boundary condition. Results generated are presented in the form of streamline, isotherm, local Nu distributions and midwidth U-velocity and temperature profiles. In addition, maximum stream function estimates and average Nu values are tabulated in Tables 1–5. Also included, for the purpose of easily assessing and quantifying the effects of baffles, are results in nonpartitioned trapezoidal cavities. Since these were given a lengthy discussion in [17], they will only be used here as a basis for comparison.

Summertime Boundary Conditions

Streamlines and isotherms. The flow and temperature fields in a nonpartitioned enclosure are displayed in Figure 2 for values of Ra ranging from 10^4 to 10^7. As shown, the flow consists of one recirculating cell with its center close to the hot wall; this center moves closer toward the lower corner of the hot wall as the Ra increases (Figure 2(a)–2(d)). Isotherms presented in Figure 2(e)–2(h) indicate dominant conduction effect at low Ra, with convection effects becoming increasingly important as Ra increases. A stratified region can be seen along the inclined surface with stratification increasing at higher Ra. At Ra $= 10^7$, more than half of the upper enclosure is stratified.

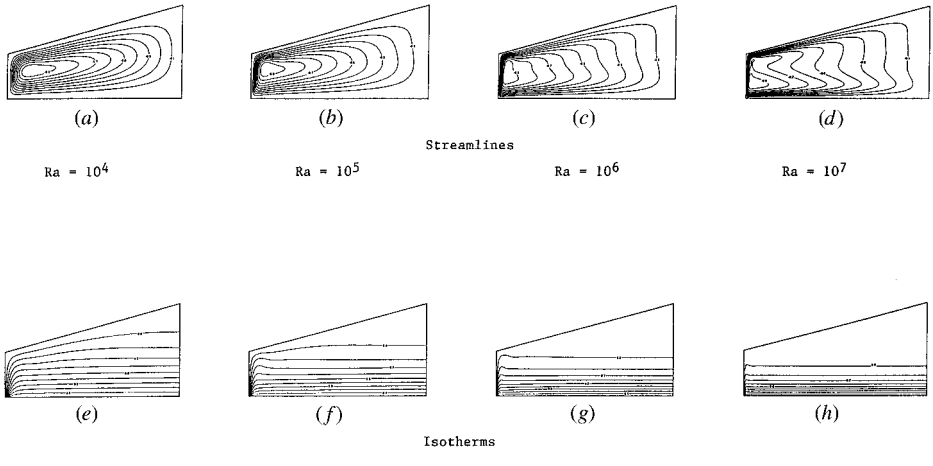

Figure 2. Streamline and isotherm plots in a nonpartitioned cavity (summer).

The influence of dividers on the flow patterns and temperature distributions are depicted in Figure 3 for $BL = W/3$ and $BH = 2H/3$ and in Figure 4 for $BL = 2W/3$ and $BH = H/3$. Streamlines presented in Figure 3 indicate that, at the lowest Ra considered ($Ra = 10^4$), the flow consists of two recirculating eddies rotating clockwise with air moving up along the heated walls and the right face of the divider, and down along the right-symmetry line and the left face of the divider. There appears to be very little communication between the flow in the two halves of the enclosure. At this low Ra, the flow to the left of the baffle is not sufficiently buoyant to penetrate into the right portion of the domain. As the Ra increases, the flow is stronger and there is greater exchange of fluid between the left and right parts of the enclosure. This exchange is facilitated primarily by a thin layer circulating adjacent to the bounding walls of the cavity and around the divider. At the higher Ras, as the heated flow negotiates the turning around the baffle tip, it encounters the stratified region in the upper-right region of the enclosure (see isotherm plots) and separates forming a jet stream directed from the baffle tip to the symmetry plane. The higher the Ra, the greater is the flow stratification in the upper-right half and more of the flow separates near the tip. This flow separation produces the two-cell pattern in the right half in Figures 3(*b*)–(*d*). At $Ra = 10^6$ and 10^7, the strong flow separation at the tip leads to the separated flow impinging on the symmetry plane and then turned downward and to the left toward the heated wall. Thus at these high Ras, there is strong flow communication between the left half of the enclosure and the lower-right half.

Isotherms displayed in Figure 3(*e*) ($Ra = 10^4$) are uniformly distributed over the domain indicating conduction as the important heat transfer mode. As Ra increases (Figures 3(*f*)–3(*h*)), convection is promoted, isotherms are more distorted, and the upper-right part of the enclosure has a homogeneous temperature and is thermally stratified. Moreover, isotherms are concentrated along the cold base of the cavity indicating strong convection induced flows along the base.

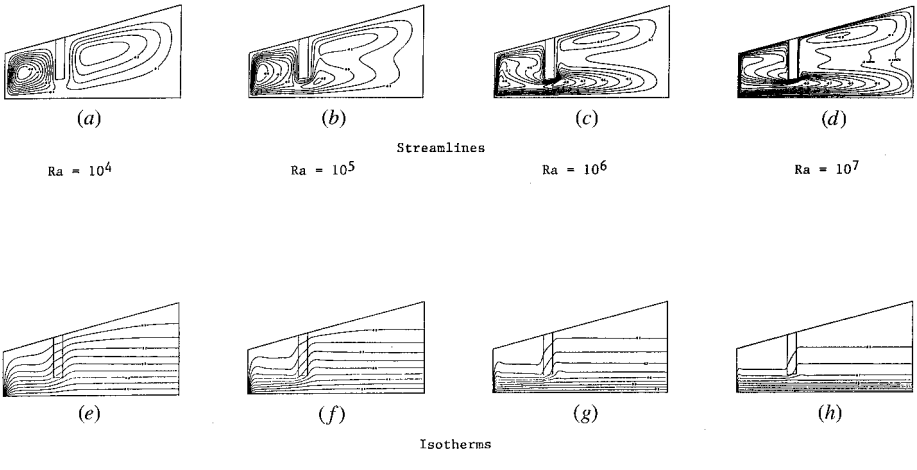

Figure 3. Streamline and isotherm plots for $BL = W/3$ and $BH = 2H/3$ (summer).

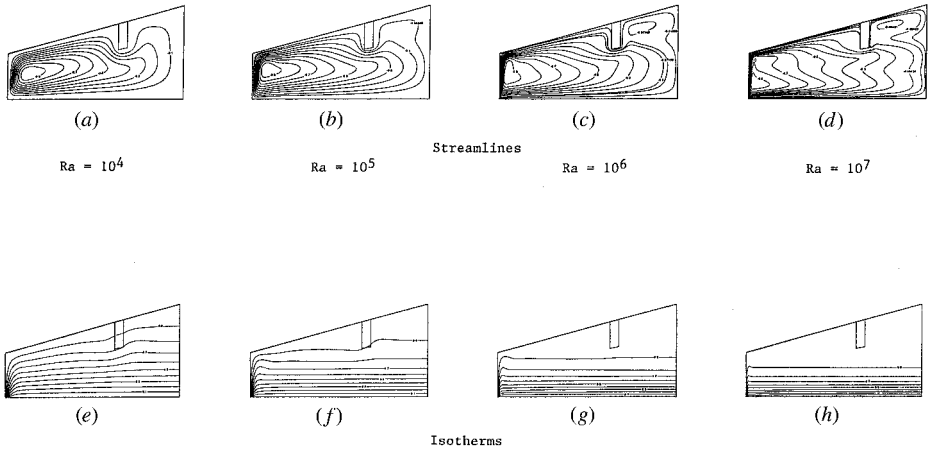

Figure 4. Streamline and isotherm plots for BL $= 2W/3$ and BH $= H/3$ (summer).

Comparing the isotherm patterns in Figures 2 and 3, it would appear that the baffles lead to higher stratification levels to the left of the divider and lower stratification levels to the right.

The effects of using a shorter divider (BH $= H/3$) placed closer to the symmetry line (BL $= 2W/3$) on the flow and temperature fields are depicted in Figure 4. Unlike the streamline maps presented in Figure 3, at low values of Ras (Ra $= 10^4$ and 10^5), the flow consists of one eddy rotating clockwise. This is because the flow between the divider and the symmetry line is not highly stratified to inhibit the penetration of the flow descending into the divider (see Figure 4(e)). Further, since the baffle is placed closer to the symmetry plane, the heated surface area left of the baffle is greater and the flow in the left half is more buoyant than the case shown in Figure 3. As Ra increases, the flow in the upper regions, and particularly in the upper-right half, becomes increasingly stratified (see isotherm patterns in Figures 4(g) and 4(h)), and this makes flow penetration into the upper-right half more difficult. At high Ra values, the flow behaves essentially as discussed earlier with flow separating near the baffle tip.

Table 1 lists the maximum stream function value for all the cases studied. It is noted that at low Ras, the presence of baffles reduces the flow strength as expected. However, at the highest Ra studied, the maximum stream function value for the baffled enclosures is higher. This is associated with the strong flow separation from the baffle tip, which augments the strength of the recirculation in the left half plane. This effect is expectedly stronger for the longer baffle. Regarding the effect of baffle placement, the flow is generally stronger when the baffle is placed closer to the symmetry plane. This is because the flow in the left half encounters a greater length of the heated inclined surface when the baffle is placed closer to the symmetry plane and therefore experiences greater buoyancy-induced acceleration.

Table 1. Maximum absolute values of the stream function for summertime boundary conditions

	BH = 0	BH = $H/3$	BH = $H/3$	BH = 2 $H/3$	BH = 2 $H/3$
Ra	BL = 0	BL = $W/3$	BL = 2 $W/3$	BL = $W/3$	BL = 2 $W/3$
10^3	1.42	1.09	0.77	0.94	0.68
10^4	5.66	4.60	4.78	3.75	4.36
10^5	11.61	10.31	11.42	7.76	10.59
10^6	17.02	17.31	17.14	13.83	16.26
10^7	23.45	23.54	23.50	24.11	23.67
5×10^7	27.63	27.71	27.66	29.61	30.03

Velocity and temperature profiles. Figures 5 and 6 show, respectively, the horizontal velocity and temperature distributions at $X = W/2H$ (midway between the left wall and the right symmetry plane) for a nonpartitioned and a partitioned (BL = $W/3$, BH = $2H/3$) enclosure for different values of Ra. The profiles reflect the flow fields presented in Figures 2 and 3. At high Ra and because of lower stratification effects, the velocity profiles near the inclined top wall are steeper in the partitioned enclosure as compared with those in the nonparitioned enclosure. The same is true near the cold wall, where, for the partitioned cavity, the flow between the divider and the cold walls forms a jet directed from the tip of the baffle to the symmetry line. The high velocities associated with the separated jet can be seen clearly at Ra = 10^7 in Figure 5 at a Y location near 0.4. The temperature profiles (Figure 6) reflect the higher stratification effects near the top wall at higher Ra values. For a partitioned cavity, the stratification effects are less, and the temperature gradients are higher near the top inclined wall and lower near the cold wall as compared with those obtained in a baffle-free cavity. However, the reduction in stratification (reduced temperature gradients) near the cold wall are

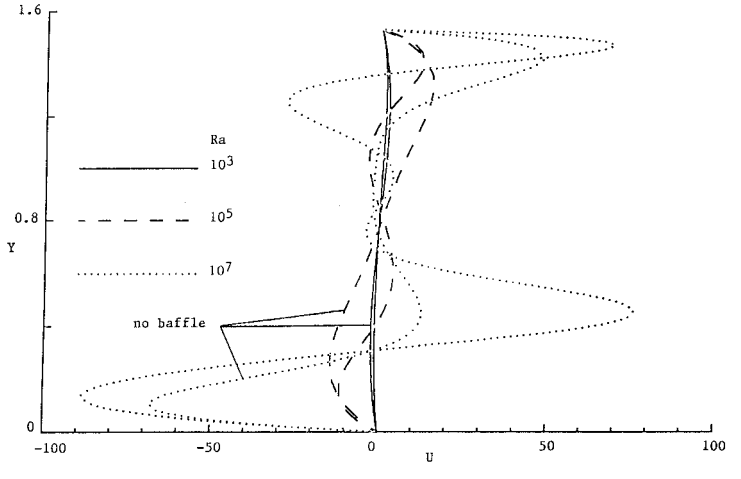

Figure 5. Velocity profiles at $X = W/2H$ for BL = $W/3$ and BH = $2H/3$ (summer).

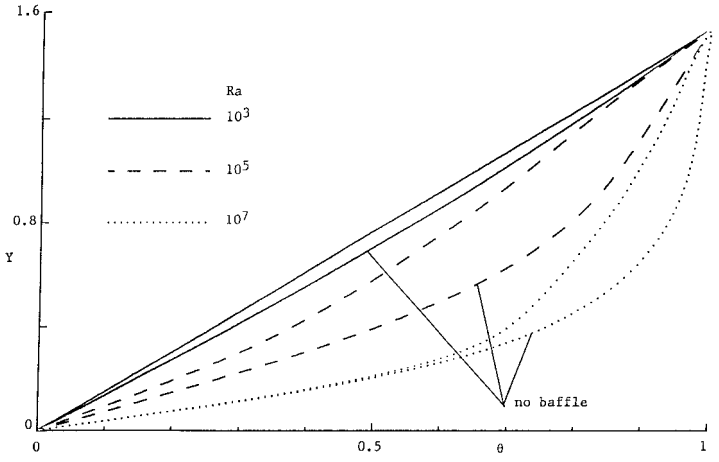

Figure 6. Temperature profiles at $X = W/2H$ for BL $= W/3$ and BH $= 2H/3$ (summer).

counteracted by the fact that as the Ra is increased, the separated jet flow becomes stronger and leads to higher velocities and higher temperature gradients near the cold wall. At Ra $= 10^7$ the gradients along the cold wall are nearly equal for both the partitioned and the nonpartitioned enclosure.

Nusselt numbers. Attention now will be focused on the effect of baffles on the total heat transfer. This will be done by presenting the average Nu for all cases under consideration (Tables 2 and 3) and by plotting the local Nu distribution along the hot upper walls and cold lower base for a partitioned and nonpartitioned

Table 2. Normalized average Nusselt number values ($\overline{\text{Nu}^*}$) for summertime boundary conditions

	BH $= 0$	BH $= H/3$	BH $= H/3$	BH $= 2\ H/3$	BH $= 2\ H/3$
Ra	BL $= 0$	BL $= W/3$	BL $= 2\ W/3$	BL $= W/3$	BL $= 2\ W/3$
10^3	1.010	1.008	1.003	1.007	1.002
10^4	1.107	1.079	1.077	1.061	1.067
10^5	1.307	1.286	1.298	1.190	1.262
10^6	1.659	1.644	1.649	1.542	1.621
10^7	2.191	2.172	2.177	2.111	2.155
5×10^7	2.519	2.500	2.504	2.428	2.479

Table 3. Average conduction Nusselt number values ($\overline{\text{Nu}^*}$) for summer- and wintertime boundary conditions

BH $= 0$	BH $= H/3$	BH $= H/3$	BH $= 2H/3$	BH $= 2H/3$
BL $= 0$	BL $= W/3$	BL $= 2W/3$	BL $= W/3$	$BL = 2W/3$
5.49204	5.53222	5.52611	5.58373	5.56718

enclosure (Figures 7 and 8). The local and average Nu along the hot and cold walls are computed using the following relations:

$$\mathrm{Nu}_h = -\frac{\left.\dfrac{\partial T}{\partial n}\right|_h S_{h,\max}}{[T_h - T_c]} \qquad \mathrm{Nu}_c = -\frac{\left.\dfrac{\partial T}{\partial n}\right|_c S_{c,\max}}{[T_h - T_c]} \tag{10}$$

$$\overline{\mathrm{Nu}_h} = \frac{1}{S_{h,\max}} \int_0^{S_{h,\max}} \mathrm{Nu}_h \, ds \qquad \overline{\mathrm{Nu}_c} = \frac{1}{S_{c,\max}} \int_0^{S_{c,\max}} \mathrm{Nu}_c \, ds \tag{11}$$

where n denotes the normal distance from the wall, S is the distance along the wall measured from the point of intersection between the hot and cold walls, and $S_{h,\max}$ and $S_{c,\max}$ are the maximum possible lengths of the hot and cold walls, respectively. Since $\overline{\mathrm{Nu}_h} = \overline{\mathrm{Nu}_c}$ the subscript will be dropped and the average heat transfer will be denoted by $\overline{\mathrm{Nu}}$.

The normalized local Nu distributions Nu* ($\mathrm{Nu}^* = \mathrm{Nu}/\mathrm{Nu}_o$, where Nu_o is the value of Nu for pure conduction; i.e., $\mathrm{Ra} = 0$) along the hot and cold walls are presented for a partition-free enclosure and a partitioned enclosure ($\mathrm{BL} = W/3$ and $\mathrm{BH} = 2H/3$) in Figures 7 and 8, respectively. In this normalized form, the relative effect of convection can be assessed directly. Values are plotted as a function of $S/S_{\max}$ where $S_{\max}$ is the maximum possible value of S along the wall.

In Figure 7, the variations of Nu* along the hot wall are displayed. At low Ra, conduction is the dominant heat transfer mode in the whole enclosure ($\mathrm{Nu}_h^* \approx 1$). At high Ra and along the vertical portion of the hot wall (i.e., $S_h/S_{h,\max} < 0.1945$) convection is the dominant heat transfer mode ($\mathrm{Nu}_h^* > 1$) for both the partitioned and nonpartitioned enclosures and Nu_h^* increases with increasing Ra values. Along the inclined portion of the hot wall ($1 > S_h/S_{h,\max} > 0.1945$), $\mathrm{Nu}_h^* < 1$ along most

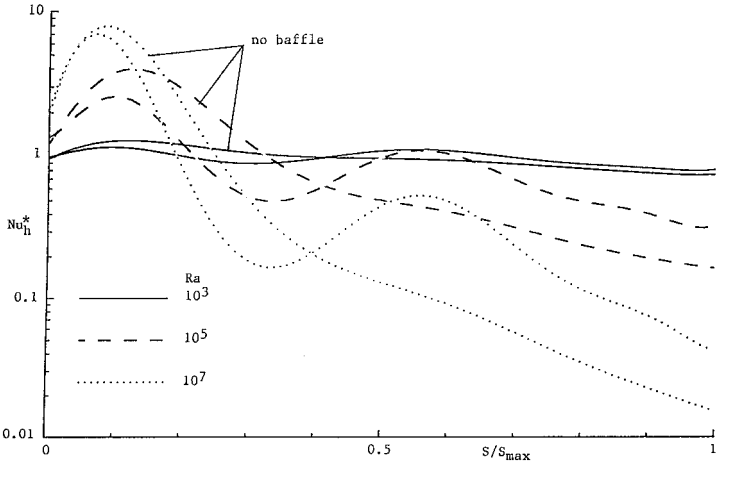

Figure 7. Local normalized Nusselt number distribution along the hot wall for $\mathrm{BL} = W/3$ and $\mathrm{BH} = 2H/3$ (summer).

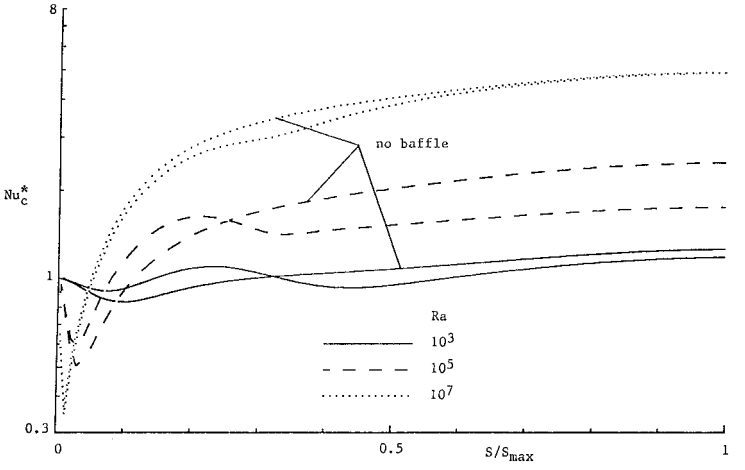

Figure 8. Local normalized Nusselt number distribution along the cold wall for BL = $W/3$ and BH = $2H/3$ (summer).

of its length and this is caused by the strong stratification effects in the upper region. As shown in Figure 7, the Nu ratio decreases all the way to the apex of the enclosure reaching values as low as 0.02.

In the presence of baffles, heat transfer along the portion of the hot wall to the left of the divider (i.e., the vertical wall and a portion of the inclined top wall) is decreased. However, the opposite is true along the remaining right portion. This decrease and increase in heat transfer is because of an increase and decrease in thermal stratification in the respective parts of the domain as reflected by the isotherms displayed in Figures 2 and 3, respectively. It is noted further that at the highest Ra presented, heat transfer nearly is unaffected by the presence of the divider over almost half of the hot vertical wall because of the strong developing boundary layer along the lower half of this wall.

The Nu distributions along the horizontal cold wall are displayed in Figure 8. As expected, the level of Nu increases with increasing Ra value. In a baffle-free enclosure, the values of Nu decrease monotonically from right to left along the cold wall since the flow is from right to left. At low and moderate Ra values, heat transfer in the partitioned enclosure is lower along the right portion of the horizontal cold wall and higher in the region close to the hot vertical wall compared with the values obtained in a baffle-free enclosure. This is caused by the lower and higher stratification levels in the right and left portions of the partitioned enclosure, respectively. At the highest Ra, the variations in Nu_c^* are similar in both enclosures with its level being slightly lower in the presence of dividers.

The normalized average Nu values ($\overline{Nu^*}$) and the average conduction values ($\overline{Nu_o}$) for all cases studied are given in Tables 2 and 3, respectively. At low and moderate Ra, the overall heat transfer appears to be dominated strongly by conduction. Convection contribution to heat transfer starts to be of importance at Ra values between 10^6 and 10^7. In general, the presence of the baffles decreases heat transfer. The rate of decrease, however, increases with increasing BH (baffle

height) and decreasing BL (distance from the hot vertical wall). Moreover, by comparing $\overline{Nu^*}$ values obtained in this study with results reported in [17] for a partitioned trapezoidal cavity with baffles attached to its cold horizontal base, the current estimates are higher with the maximum decrease in $\overline{Nu^*}$ for this configuration being about 8.95%, whereas for the configuration in [17] the corresponding decrease is 19.25%. Thus, for summertime boundary conditions, it is better to attach dividers to the cold horizontal base of the cavity if reduction in the heat transfer from one cavity to the other is the desired objective.

The average Nu values, displayed in normalized form in Table 2, are correlated with a maximum deviation less than ± 13.28% via the following relation:

$$\overline{Nu} = 2.7817(Ra)^{0.0886}\left(1 + \frac{BL}{W}\right)^{0.0189}\left(1 + \frac{BH}{H}\right)^{0.0788} \tag{13}$$

Wintertime Boundary Conditions

Streamlines and isotherms. Representative flow and thermal fields in a partitioned and a nonpartitioned enclosure for wintertime boundary conditions are presented in Figures 9–11. For this boundary condition, Lam et al. [11] have shown that a two-dimensional model cannot accurately resolve the three-dimensional flows that occur in the cavity but can predict heat transfer rates to an acceptable accuracy. Since the intention here is to estimate and correlate heat transfer, the two-dimensional model employed is perhaps sufficient.

Streamlines and isotherms displayed in Figure 9 indicate that convection is the dominant heat transfer mode in a nonpartitioned trapezoidal cavity at Ra greater than 10^3, and that the flow is composed of three convective cells with the middle one rotating clockwise. The isotherms clearly indicate rising and descending thermal plumes from the hot and cold surfaces, respectively.

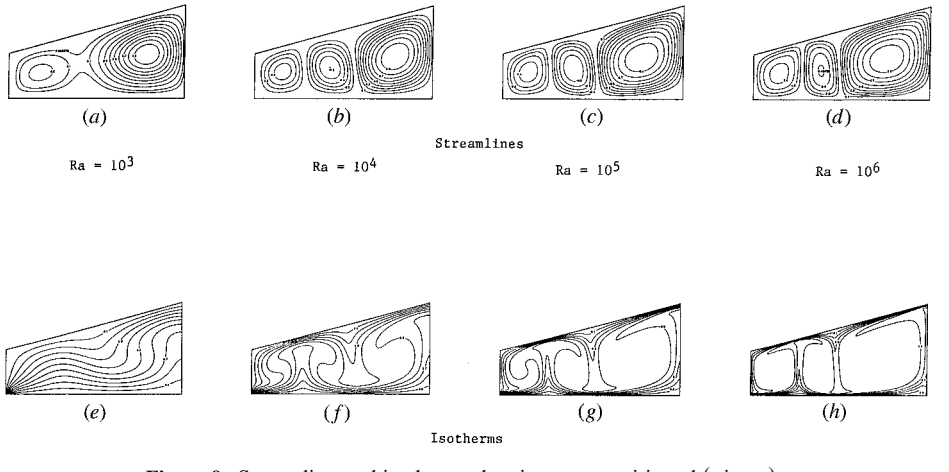

Figure 9. Streamline and isotherm plots in a nonpartitioned (winter).

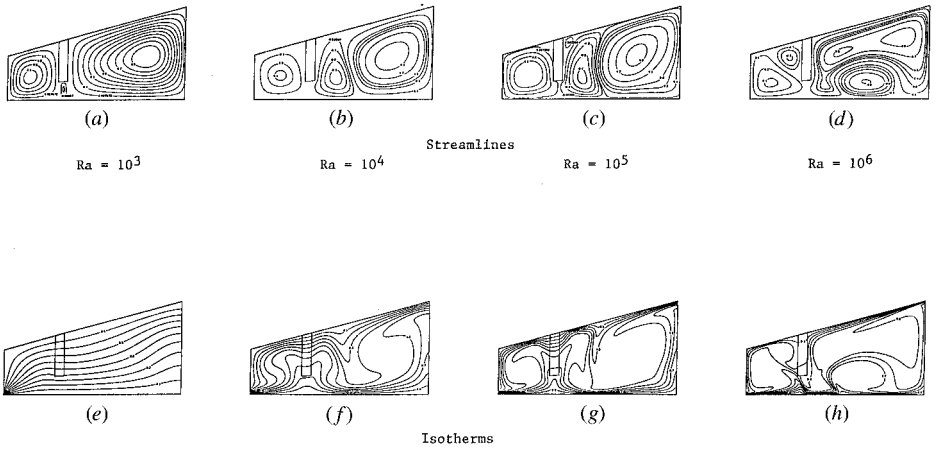

Figure 10. Streamline and isotherm plots for BL $= W/3$ and BH $= 2H/3$ (winter).

Results in Figure 10 are for a partitioned cavity with long baffles (BH $= 2H/3$) located away from the symmetry line (BL $= W/3$), whereas those in Figure 11 are for short baffles (BH $= H/3$) placed close to the symmetry line (BL $= 2W/3$). At low Ra, the presence of the dividers does not grossly distort the flow pattern. The two-roll pattern at Ra $= 10^3$ and the three-roll pattern at Ra $= 10^4$ are both preserved. However, at the higher Ra (Ra $\geq 10^5$) the presence of the dividers greatly affects the flow and temperature fields, and the presence of secondary roll cells can be observed. At all Ra, there is little communication between the two sides.

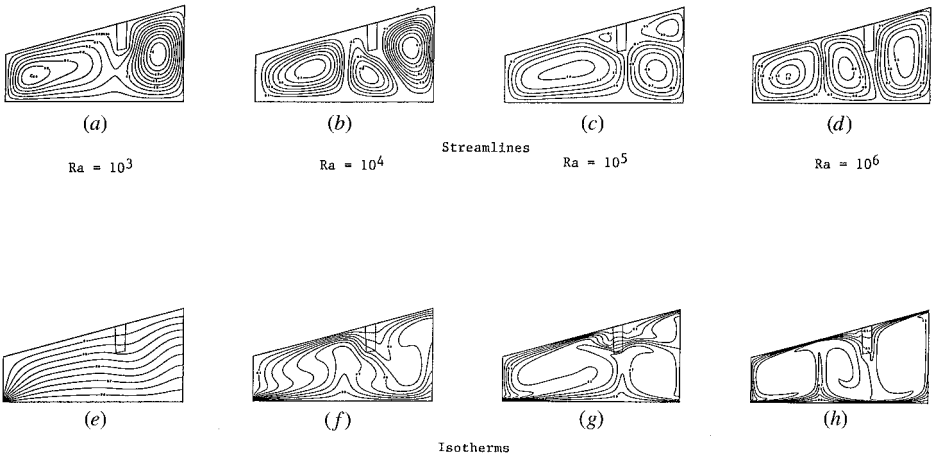

Figure 11. Streamline and isotherm plots for BL $= 2W/3$ and BH $= H/3$ (winter).

Table 4. Maximum absolute values of the stream function for wintertime boundary conditions

	BH = 0	BH = $H/3$	BH = $H/3$	BH = $2H/3$	BH = $2H/3$
Ra	BL = 0	BL = $W/3$	BL = $2W/3$	BL = $W/3$	BL = $2W/3$
10^3	7.72	1.97	1.67	2.00	1.55
10^4	35.15	28.87	21.74	28.86	21.74
10^5	107.97	84.65	59.94	98.96	64.40
10^6	318.35	217.60	178.52	181.87	183.34

The effect of baffles on the strength of the flow established within the cavity is quantitatively presented in Table 4 through the maximum absolute values of the stream function ($|\Psi_{max}|$). The lowest values obtained are for the configurations in which baffles are placed close to the symmetry line. Moreover, at the higher values of Ra ($Ra \geq 10^4$), the lowest ($|\Psi_{max}|$) values are generally obtained for the case when BL = $2W/3$ and BH = $H/3$.

Velocity and temperature profiles. The horizontal velocity components at different values of Ra, along $X = W/2H$, are displayed in Figure 12 for a nonpartitioned enclosure and a partitioned one with a divider of height BH = $H/3$ located at BL = $2W/3$. The significant effect of the baffles can be noted at $Ra = 10^6$ where the flow directions on the top and bottom walls are opposite to each other for the baffled and unbaffled cases. Such differences are because of the relative locations of the clockwise and counterclockwise eddies in the two cases. A similar behavior is observed at the lower Ras, although the velocity magnitudes are considerably lower.

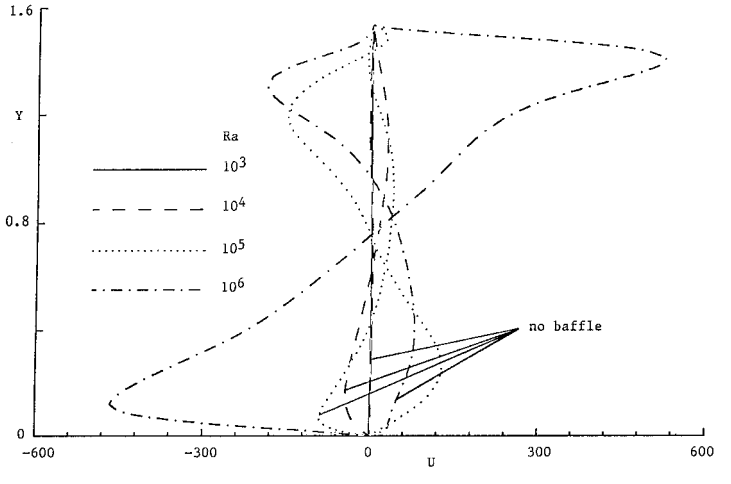

Figure 12. Velocity profiles at $X = W/2H$ for BL = $2W/3$ and BH = $H/3$ (winter).

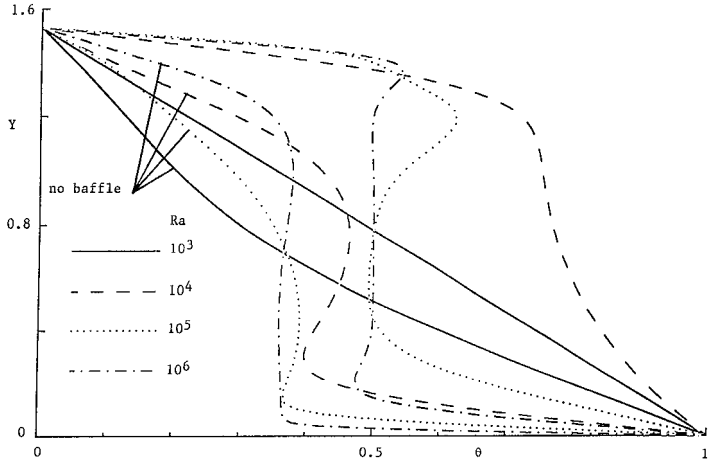

Figure 13. Temperature profiles at $X = W/2H$ for BL $= 2W/3$ and BH $= H/3$ (winter).

The temperature profiles (Figure 13) across the midwidth ($X = W/2H$) for the same partitioned and nonpartitioned enclosures reflect the isotherm maps presented in Figures 9 and 11. At low Ra, a linear variation in the temperature is obtained indicating dominant conduction heat transfer. At high Ra, however, the temperature profiles reveal high gradients close to the hot and cold walls characterizing thermal boundary layers and low core temperature gradients indicating stratification in the core. This is more pronounced in a partitioned enclosure. Furthermore, at high Ra values, there is clear evidence of temperature inversion both near the hot and cold walls. As in the velocity profiles, partitions produce substantial differences in the temperature profiles. For example, both at Ra $= 10^5$ and 10^6, the enclosure with no baffles has lower thermal gradients along the top wall at $X = W/2H$. With baffles, the situation is reversed, with higher temperature gradients along the top wall. These dramatic differences again are linked to the fact that the baffles influence the relative locations of the plumes and thus influence the location of the large thermal gradients along the top and bottom walls.

Nusselt numbers. The local and average Nu along the hot and cold walls are computed using Eqs. (10) and (11), respectively. As for the summertime boundary conditions, estimates are normalized with respect to the pure conduction values. The effects on heat transfer of mounting baffles to the upper inclined plane of the cavity can be assessed by a direct comparison between the normalized local Nu distributions Nu* along the hot and cold walls of a nonpartitioned and a partitioned enclosure (BL $= 2W/3$ and BH $= H/3$) and are displayed in Figures 14 and 15, respectively. Along the hot wall of a nonpartitioned enclosure (Figure 14), the same trend is observed at all values of Ra considered, with an increase in the level of Nu* with increasing Ra. As depicted, a dual peak in the normalized Nu is noticed. These peak locations represent the position where the thermal plume impinges on the surface. In the presence of baffles, the level of Nu* for the same

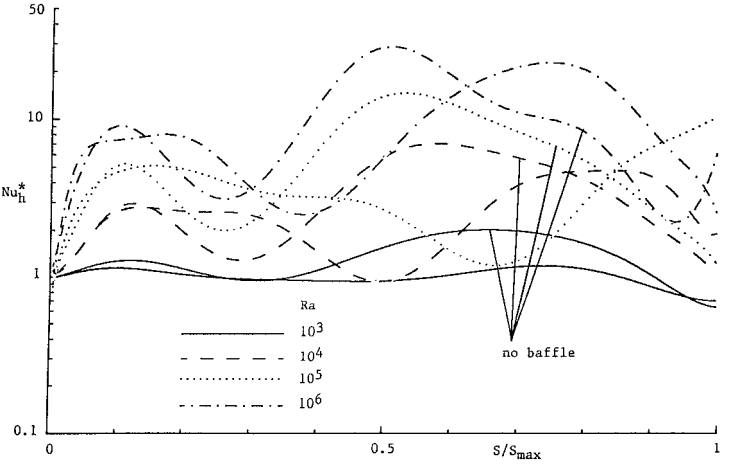

Figure 14. Local normalized Nusselt number distribution along the hot wall for BL = $2W/3$ and BH = $H/3$ (winter).

value of Ra decreases, indicating a decrease in the heat transfer because of the baffles. At Ra = 10^3, 10^4, and 10^6, because of a similarity of the flow pattern with that in a partition-free enclosure, the Nu* distributions in the partitioned enclosure are similar to those in a nonpartitioned enclosure. The differences are that with partitions there is a decrease in the Nu levels and a change in the locations where they peak because of a shift in the locations of the thermal plumes induced by the baffles. The peaks in the partitioned enclosure are flatter than in a

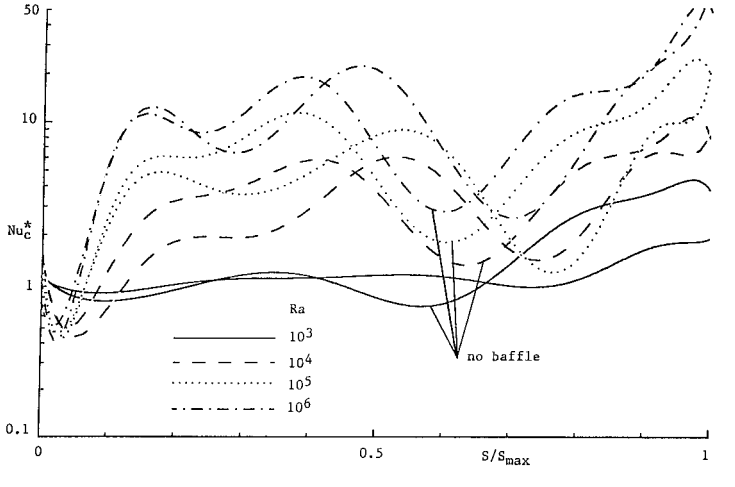

Figure 15. Local normalized Nusselt number distribution along the cold wall for BL = $2W/3$ and BH = $H/3$ (winter).

nonpartitioned cavity because of lower plume strength. At $Ra = 10^5$, a local decrease in Nu* directly below the divider is observed for the partitioned enclosure. This local minimum is again linked to a thermal plume directed away from the minimum-Nu location (Figure 11*g*). The upward-directed plume corresponds to the location where the right-clockwise rotating eddy meets the left-counterclockwise rotating eddy, and the flow is directed upward as a plume toward the divider.

The normalized Nu distributions along the cold wall are displayed in Figure 15. In a baffle-free enclosure, the Nu distribution corresponds to the three-roll pattern. Thus there are two local impingement peaks corresponding to the two smaller roll cells, followed by a minimum between the large and the intermediate roll cells where the plume is directed upward. In the presence of baffles, the Nu distribution is influenced by the changes in the flow field. The general effect of the baffle is to shift the second peak toward the baffle and to accentuate it, followed by a local minimum (depression) in Nu* immediately beyond the baffle.

The heat transfer results, presented in the form of average normalized Nu values in Table 5, reveal that convection becomes important at relatively low values of the Ra. Moreover, as for the summertime boundary condition, partitioning the domain decreases the overall heat transfer. In general, for a given BH, the rate of decrease increase with increasing distance from the vertical wall (BL). The highest decrease in heat transfer is obtained with the longest baffle ($BH = 2H/3$) placed close to the symmetry line ($BL = 2W/3$). A comparison between current $\overline{Nu^*}$ estimates and those reported in [17] reveals that, in general, with a wintertime boundary condition it is better to attach baffles to the upper inclined plane of the cavity, rather than to its lower base. The maximum decrease in $\overline{Nu^*}$ for this configuration is about 34.00%, whereas for the configuration in [17] the corresponding decrease is 31.51%, both obtained at $Ra = 10^5$ in a partitioned cavity with a baffle height $BH = 2H/3$ located at $BL = 2W/3$.

The average Nu values, displayed in normalized form in Table 5, are correlated as

$$\overline{Nu} = 1.3967(Ra)^{0.2346}\left(1 + \frac{BL}{W}\right)^{-0.1089}\left(1 + \frac{BH}{H}\right)^{-0.1717} \tag{14}$$

with a maximum deviation of less than ± 11.3%.

Table 5. Normalized average Nusselt number values ($\overline{Nu^*}$) for wintertime boundary conditions

	BH = 0	BH = $H/3$	BH = $H/3$	BH = 2 $H/3$	BH = 2 $H/3$
Ra	BL = 0	BL = $W/3$	BL = 2 $W/3$	BL = $W/3$	BL = 2 $W/3$
10^3	1.185	1.027	1.020	1.029	1.018
10^4	2.317	2.082	1.932	2.004	1.850
10^5	4.055	3.239	2.794	3.399	2.676
10^6	6.360	5.862	5.990	4.827	4.688

CLOSING REMARKS

Natural convection in a trapezoidal cavity with baffles mounted to its upper inclined plane has been studied numerically. In particular, the effects of Ra, BH, and BL on heat transfer in summerlike (bottom-cooled) and winterlike (bottom-heated) conditions are investigated. For both boundary conditions, convection contribution to total heat transfer is found to increase with increasing Ra. Nevertheless, convection is far more pronounced in wintertime conditions. For bottom-cooled situations, the presence of baffles decreases heat transfer, with the heat transfer rate decreasing with increasing BH and increasing BL (distance of the baffle from the vertical wall). However, baffles decrease the thermal stratification in the upper midregions (between the baffle and the centerplane) of the enclosure. For bottom-heated conditions, and for a given BH, the heat transfer rate increases with increasing distance from the vertical wall (BL). By comparing current estimates with those presented in [17] for the case when the divider is attached to the lower base of the cavity, it is found that for summerlike conditions it is better to mount the baffle to the lower base of the cavity, whereas for winterlike conditions the opposite holds.

REFERENCES

1. S. Ostrach, Natural Convection in Enclosures, *Journal of Heat Transfer*, vol. 110, pp. 1175–1190, 1988.
2. V. A. Akinsete and T. A. Coleman, Heat Transfer by Steady Laminar Free Convection in Triangular Enclosures, *Int. J. Heat Mass Transfer*, vol. 25, no. 7, pp. 991–998, 1982.
3. YU. E. Karyakin, YU. A. Sokovishin, and O. G. Martynenko, Transient Natural Convection in Triangular Enclosures, *Int. J. Heat Mass Transfer*, vol. 31, no. 9, pp. 1759–1766, 1988.
4. A. Bejan and D. Poulikakos, Natural Convection in an Attic Shaped Space Filled with Porous Material, *Journal of Heat Transfer*, vol. 104, pp. 241–247, 1982.
5. D. Poulikakos and A. Bejan, The Fluid Dynamics of an Attic Space, *Journal of Fluid Mechanics*, vol. 131, pp. 251–269, 1983.
6. D. Poulikakos and A. Bejan, Natural Convection in a Triangular Enclosure, *Journal of Heat Transfer*, vol. 105, pp. 652–655, 1983.
7. H. Salmun, Convection Patterns in a Triangular Domain, *Int. J. Heat Mass Transfer*, vol. 38, no. 2, pp. 351–362, 1995.
8. H. Salmun, The Stability of a Single-Cell Steady-State Solution in a Triangular Enclosure, *Int. J. Heat Mass Transfer*, vol. 38, no. 2, pp. 363–369, 1995.
9. L. Iyican, Y. Bayazitoglu, and L. Witte, An Analytical Study of Natural Convection Heat Transfer within a Trapezoidal Enclosure, *Journal of Heat Transfer*, vol. 102, pp. 640–647, 1980.
10. L. Iyican, L. C. Witte, and Y. Bayazitoglu, An Experimental Study of Natural Convection in Trapezoidal Enclosures, *Journal of Heat Transfer*, vol. 102, pp. 648–653, 1980.
11. S. W. Lam, R. Gani, and J. G. Symons, Experimental and Numerical Studies of Natural Convection in Trapezoidal Cavities, *Journal of Heat Transfer*, vol. 111, pp. 372–377, 1989.
12. Yu. E. Karyakin, Transient Natural Convection in Prismatic Enclosures of Arbitrary Cross-Section, *Int. J. Heat Mass Transfer*, vol. 32, no. 6, pp. 1095–1103, 1989.
13. T. S. Lee, Numerical Experiments with Fluid Convection in Tilted Nonrectangular Enclosures, *Numerical Heat Transfer, Part A*, vol. 19, pp. 487–499, 1991.

14. M. Peric, Natural Convection in Trapezoidal Cavities, *Numerical Heat Transfer*, *Part A*, vol. 24, pp. 213–219, 1993.
15. H. Sadat and P. Salagnac, Further Results for Laminar Natural Convection in a Two-Dimensional Trapezoidal Enclosure, *Numerical Heat Transfer*, *Part A*, vol. 27, pp. 451–459, 1995.
16. R. A. Kuyper and C. J. Hoogendoorn, Laminar Natural Convection Flow in Trapezoidal Enclosures, *Numerical Heat Transfer*, *Part A*, vol. 28, pp. 55–67, 1995.
17. F. Moukalled and S. Acharya, Buoyancy-Induced Heat Transfer in Partially Divided Trapezoidal Cavities, *Numerical Heat Transfer*, *Part A*, in press.
18. C. M. Rhie and W. L. Chow, Numerical Study of the Turbulent Flow Past an Airfoil with Trailing Edge Separation, *AIAA Journal*, vol. 21, pp. 1525–1532, 1983.
19. S. V. Patankar, *Numerical Heat Transfer and Fluid Flow*, Hemisphere, New York, 1980.
20. W. J. Gordon and C. A. Hall, Construction of Curvilinear Coordinate Systems and Applications to Mesh Generation, *Int. J. Numer. Methods Eng.*, vol. 7, pp. 461–477, 1973.
21. W. J. Gordon and L. C. Theil, Tranfinite Mappings and Their Applications to Grid Generation, in J. F. Thopmson (ed.), *Numerical Grid Generation*, North Holland, New York, pp. 171–192, 1982.
22. R. Haber, M. S. Shephard, J. F. Abel, R. H. Gallagher, and D. P. Grennberg, A General Two-Dimensional, Graphical Finite Element Pre-Processor Utilizing Discrete Transfinite Mappings, *Int. J. Numer. Methods Eng.*, vol. 17, pp. 1015–1044, 1981.